Demonstration of Ignition Radiation Temperatures in Indirect-Drive Inertial Confinement Fusion Hohlraums

S. H. Glenzer,[1] B. J. MacGowan,[1] N. B. Meezan,[1] P. A. Adams,[1] J. B. Alfonso,[1] E. T. Alger,[1] Z. Alherz,[1] L. F. Alvarez,[1]
S. S. Alvarez,[1] P. V. Amick,[1] K. S. Andersson,[1] S. D. Andrews,[1] G. J. Antonini,[1] P. A. Arnold,[1] D. P. Atkinson,[1] L. Auyang,[1]
S. G. Azevedo,[1] B. N. M. Balaoing,[1] J. A. Baltz,[1] F. Barbosa,[1] G. W. Bardsley,[1] D. A. Barker,[1] A. I. Barnes,[1] A. Baron,[1]
R. G. Beeler,[1] B. V. Beeman,[1] L. R. Belk,[1] J. C. Bell,[1] P. M. Bell,[1] R. L. Berger,[1] M. A. Bergonia,[1] L. J. Bernardez,[1]
L. V. Berzins,[1] R. C. Bettenhausen,[1] L. Bezerides,[1] S. D. Bhandarkar,[1] C. L. Bishop,[1] E. J. Bond,[1] D. R. Bopp,[1]
J. A. Borgman,[1] J. R. Bower,[1] G. A. Bowers,[1] M. W. Bowers,[1] D. T. Boyle,[1] D. K. Bradley,[1] J. L. Bragg,[1] J. Braucht,[1]
D. L. Brinkerhoff,[1] D. F. Browning,[1] G. K. Brunton,[1] S. C. Burkhart,[1] S. R. Burns,[1] K. E. Burns,[1] B. Burr,[1] L. M. Burrows,[1]
R. K. Butlin,[1] N. J. Cahayag,[1] D. A. Callahan,[1] P. S. Cardinale,[1] R. W. Carey,[1] J. W. Carlson,[1] A. D. Casey,[1] C. Castro,[1]
J. R. Celeste,[1] A. Y. Chakicherla,[1] F. W. Chambers,[1] C. Chan,[1] H. Chandrasekaran,[1] C. Chang,[1] R. F. Chapman,[1]
K. Charron,[1] Y. Chen,[1] M. J. Christensen,[1] A. J. Churby,[1] T. J. Clancy,[1] B. D. Cline,[1] L. C. Clowdus,[1] D. G. Cocherell,[1]
F. E. Coffield,[1] S. J. Cohen,[1] R. L. Costa,[1] J. R. Cox,[1] G. M. Curnow,[1] M. J. Dailey,[1] P. M. Danforth,[1] R. Darbee,[1]
P. S. Datte,[1] J. A. Davis,[1] G. A. Deis,[1] R. D. Demaret,[1] E. L. Dewald,[1] P. Di Nicola,[1] J. M. Di Nicola,[1] L. Divol,[1] S. Dixit,[1]
D. B. Dobson,[1] T. Doppner,[1] J. D. Driscoll,[1] J. Dugorepec,[1] J. J. Duncan,[1] P. C. Dupuy,[1] E. G. Dzenitis,[1] M. J. Eckart,[1]
S. L. Edson,[1] G. J. Edwards,[1] M. J. Edwards,[1] O. D. Edwards,[1] P. W. Edwards,[1] J. C. Ellefson,[1] C. H. Ellerbee,[1]
G. V. Erbert,[1] C. M. Estes,[1] W. J. Fabyan,[1] R. N. Fallejo,[1] M. Fedorov,[1] B. Felker,[1] J. T Fink,[1] M. D. Finney,[1] L. F. Finnie,[1]
M. J. Fischer,[1] J. M. Fisher,[1] B. T. Fishler,[1] J. W. Florio,[1] A. Forsman,[1] C. B. Foxworthy,[1] R. M. Franks,[1] T. Frazier,[1]
G. Frieder,[1] T. Fung,[1] G. N. Gawinski,[1] C. R. Gibson,[1] E. Giraldez,[1] S. M. Glenn,[1] B. P. Golick,[1] H. Gonzales,[1]
S. A. Gonzales,[1] M. J. Gonzalez,[1] K. L. Griffin,[1] J. Grippen,[1] S. M. Gross,[1] P. H. Gschweng,[1] G. Gururangan,[1] K. Gu,[1]
S. W. Haan,[1] S. R. Hahn,[1] B. J. Haid,[1] J. E. Hamblen,[1] B. A. Hammel,[1] A. V. Hamza,[1] D. L. Hardy,[1] D. R. Hart,[1]
R. G. Hartley,[1] C. A. Haynam,[1] G. M. Heestand,[1] M. R. Hermann,[1] G. L. Hermes,[1] D. S. Hey,[1] R. L. Hibbard,[1]
D. G. Hicks,[1] D. E. Hinkel,[1] D. L. Hipple,[1] J. D. Hitchcock,[1] D. L. Hodtwalker,[1] J. P. Holder,[1] J. D. Hollis,[1]
G. M. Holtmeier,[1] S. R. Huber,[1] A. W. Huey,[1] D. N. Hulsey,[1] S. L. Hunter,[1] T. R. Huppler,[1] M. S. Hutton,[1] N. Izumi,[1]
J. L. Jackson,[1] M. A. Jackson,[1] K. S. Jancaitis,[1] D. R. Jedlovec,[1] B. Johnson,[1] M. C. Johnson,[1] T. Johnson,[1] M. P. Johnston,[1]
O. S. Jones,[1] D. H. Kalantar,[1] J. H. Kamperschroer,[1] R. L. Kauffman,[1] G. A. Keating,[1] L. M. Kegelmeyer,[1] S. L. Kenitzer,[1]
J. R. Kimbrough,[1] K. King,[1] R. K. Kirkwood,[1] J. L. Klingmann,[1] K. M. Knittel,[1] T. R. Kohut,[1] K. G. Koka,[1] S. W. Kramer,[1]
J. E. Krammen,[1] K. G. Krauter,[1] G. W. Krauter,[1] E. K. Krieger,[1] J. J. Kroll,[1] K. N. La Fortune,[1] L. J. Lagin,[1]
V. K. Lakamsani,[1] O. L. Landen,[1] S. W. Lane,[1] A. B. Langdon,[1] S. H. Langer,[1] N. Lao,[1] D. W. Larson,[1] D. Latray,[1]
G. T. Lau,[1] S. Le Pape,[1] B. L. Lechleiter,[1] Y. Lee,[1] T. L. Lee,[1] J. Li,[1] J. A. Liebman,[1] J. D. Lindl,[1] S. F. Locke,[1] H. K. Loey,[1]
R. A. London,[1] F. J. Lopez,[1] D. M. Lord,[1] R. R. Lowe-Webb,[1] J. G. Lown,[1] A. P. Ludwigsen,[1] N. W. Lum,[1] R. R. Lyons,[1]
T. Ma,[1] A. J. MacKinnon,[1] M. D. Magat,[1] D. T. Maloy,[1] T. N. Malsbury,[1] G. Markham,[1] R. M. Marquez,[1] A. A. Marsh,[1]
C. D. Marshall,[1] S. R. Marshall,[1] I. L. Maslennikov,[1] D. G. Mathisen,[1] G. J. Mauger,[1] M. -Y. Mauvais,[1] J. A. McBride,[1]
T. McCarville,[1] J. B. McCloud,[1] A. McGrew,[1] B. McHale,[1] A. G. MacPhee,[1] J. F. Meeker,[1] J. S. Merill,[1] E. P. Mertens,[1]
P. A. Michel,[1] M. G. Miller,[1] T. Mills,[1] J. L. Milovich,[1] R. Miramontes,[1] R. C. Montesanti,[1] M. M. Montoya,[1] J. Moody,[1]
J. D. Moody,[1] K. A. Moreno,[1] J. Morris,[1] K. M. Morriston,[1] J. R. Nelson,[1] M. Neto,[1] J. D. Neumann,[1] E. Ng,[1] Q. M. Ngo,[1]
B. L. Olejniczak,[1] R. E. Olson,[1] N. L. Orsi,[1] M. W. Owens,[1] E. H. Padilla,[1] T. M. Pannell,[1] T. G. Parham,[1]
R. W. Patterson, Jr.,[1] G. Pavel,[1] R. R. Prasad,[1] D. Pendlton,[1] F. A. Penko,[1] B. L. Pepmeier,[1] D. E. Petersen,[1] T. W. Phillips,[1]
D. Pigg,[1] K. W. Piston,[1] K. D. Pletcher,[1] C. L. Powell,[1] H. B. Radousky,[1] B. S. Raimondi,[1] J. E. Ralph,[1] R. L. Rampke,[1]
R. K. Reed,[1] W. A. Reid,[1] V. V. Rekow,[1] J. L. Reynolds,[1] J. J. Rhodes,[1] M. J. Richardson,[1] R. J. Rinnert,[1] B. P. Riordan,[1]
A. S. Rivenes,[1] A. T. Rivera,[1] C. J. Roberts,[1] J. A. Robinson,[1] R. B. Robinson,[1] S. R. Robison,[1] O. R. Rodriguez,[1]
S. P. Rogers,[1] M. D. Rosen,[1] G. F. Ross,[1] M. Runkel,[1] A. S. Runtal,[1] R. A. Sacks,[1] S. F. Sailors,[1] J. T. Salmon,[1]
J. D. Salmonson,[1] R. L. Saunders,[1] J. R. Schaffer,[1] T. M. Schindler,[1] M. J. Schmitt,[1] M. B. Schneider,[1] K. S. Segraves,[1]
M. J. Shaw,[1] M. E. Sheldrick,[1] R. T. Shelton,[1] M. K. Shiflett,[1] S. J. Shiromizu,[1] M. Shor,[1] L. L. Silva,[1] S. A. Silva,[1]
K. M. Skulina,[1] D. A. Smauley,[1] B. E. Smith,[1] L. K. Smith,[1] A. L. Solomon,[1] S. Sommer,[1] J. G. Soto,[1] N. I. Spafford,[1]
D. E. Speck,[1] P. T. Springer,[1] M. Stadermann,[1] F. Stanley,[1] T. G. Stone,[1] E. A. Stout,[1] P. L. Stratton,[1] R. J. Strausser,[1]
L. J. Suter,[1] W. Sweet,[1] M. F. Swisher,[1] J. D. Tappero,[1] J. B. Tassano,[1] J. S. Taylor,[1] E. A. Tekle,[1] C. Thai,[1] C. A. Thomas,[1]
A. Thomas,[1] A. L. Throop,[1] G. L. Tietbohl,[1] J. M. Tillman,[1] R. P. J. Town,[1] S. L. Townsend,[1] K. L. Tribbey,[1] D. Trummer,[1]
J. Truong,[1] J. Vaher,[1] M. Valadez,[1] P. Van Arsdall,[1] A. J. Van Prooyen,[1] E. O. Vergel de Dios,[1] M. D. Vergino,[1]

S. P. Vernon,[1] J. L. Vickers,[1] G. T. Villanueva,[1] M. A. Vitalich,[1] S. A. Vonhof,[1] F. E. Wade,[1] R. J. Wallace,[1] C. T. Warren,[1]
A. L. Warrick,[1] J. Watkins,[1] S. Weaver,[1] P. J. Wegner,[1] M. A. Weingart,[1] J. Wen,[1] K. S. White,[1] P. K. Whitman,[1]
K. Widmann,[1] C. C. Widmayer,[1] K. Wilhelmsen,[1] E. A. Williams,[1] W. H. Williams,[1] L. Willis,[1] E F. Wilson,[1]
B. A. Wilson,[1] M. C. Witte,[1] K. Work,[1] P. S. Yang,[1] B. K. Young,[1] K. P. Youngblood,[1] R. A. Zacharias,[1] T. Zaleski,[1]
P. G. Zapata,[1] H. Zhang,[1] J. S. Zielinski,[1] J. L. Kline,[2] G. A. Kyrala,[2] C. Niemann,[3] J. D. Kilkenny,[4] A. Nikroo,[4]
B. M. Van Wonterghem,[1] L. J. Atherton,[1] and E. I. Moses[1]

[1]*Lawrence Livermore National Laboratory, Livermore, California 94550, USA*
[2]*Los Alamos National Laboratory, Los Alamos, New Mexico 87545, USA*
[3]*Department of Physics and Astronomy, University of California, Los Angeles, California 90095, USA*
[4]*General Atomics, San Diego, California 92121, USA*
(Received 14 September 2010; published 25 February 2011; corrected 28 February 2011)

We demonstrate the hohlraum radiation temperature and symmetry required for ignition-scale inertial confinement fusion capsule implosions. Cryogenic gas-filled hohlraums with 2.2 mm-diameter capsules are heated with unprecedented laser energies of 1.2 MJ delivered by 192 ultraviolet laser beams on the National Ignition Facility. Laser backscatter measurements show that these hohlraums absorb 87% to 91% of the incident laser power resulting in peak radiation temperatures of $T_{\mathrm{RAD}} = 300$ eV and a symmetric implosion to a 100 μm diameter hot core.

The 192 laser beams of the National Ignition Facility (NIF) [1] have recently been commissioned [2] to deliver the laser energy and power required for heating ignition-scale hohlraums to indirect-drive inertial confinement fusion conditions. Efficient coupling of the laser beams and efficient heating of the hohlraum to radiation temperatures of 270 eV $\leq T_{\mathrm{RAD}} \leq 300$ eV are design goals for compressing the fusion capsule in the center of the hohlraum in a rocketlike spherical implosion. Ignition and significant fusion yield require centimeter-scale hohlraums that hold a 2.2 mm-diameter fusion capsule with approximately 0.17 mg of nuclear fuel. The fuel is prepared cryogenically into a solid deuterium-tritium ice layer surrounded by low-Z ablator material [3]. The hohlraum radiation field heats the ablator, generating ablation pressures in excess of 100 MBar. The rocketlike acceleration of the shell in response to this ablation pressure compresses the shell toward the center and fuel densities in excess of 1000 g/cm^3 are produced. This high density shell of fuel surrounds a hot spot which reaches temperatures in excess of 10 keV from a combination of PdV work and alpha deposition. At this point, a nuclear burn wave is launched igniting the surrounding dense fuel, sustained by alpha deposition and electron conduction without an external energy source [4–6].

Burning approximately 1/3 of the DT-fuel will result into 6.5×10^{18} fusion neutrons primarily from the $D + T = {}^4\mathrm{He}(3.5 \text{ MeV}) + n(14.1 \text{ MeV})$ process with a total yield of 15 MJ. The formation of the central hot spot and the assembly of the thermonuclear fuel requires both implosion velocities approaching 400 km/s and a symmetrically compressed capsule to a sphere with a diameter of 60 μm. At reduced scales, round implosions have been demonstrated by controlling the laser beam power on the hohlraum wall either by directly tuning the power of individual beams [7–9] or more efficiently with self-generated plasma optics gratings on the NIF [10,11]. However, implosion velocity and compression are directly related to the hohlraum radiation temperature [12–16] and thus require scaling of laser energy coupling to ignition-scale conditions.

In this letter, we present experiments of laser-heated ignition-size hohlraums with laser energies of 1.2 MJ that show 87% to 91% coupling. Losses are due to stimulated raman scattering (SRS) from the laser beams closest to the hohlraum axis that interact with the dense capsule blow-off plasma. At the megajoule level we compensate for the *local* losses and demonstrate a symmetric implosion by properly choosing the laser wavelength of the heater beams. A wavelength shift of up to 0.28 nm between the inner and outer cones of beams provides a symmetric x-ray drive by controlling the power distribution on the hohlraum wall [10,11]. In addition, the experiments indicate a population of hot (> 170 keV) electrons of $<0.1\%$ of total laser energy, and 14% gold M-band radiation fraction of x-rays in energies $E > 2$ keV. The latter is absorbed by a graded Ge dopant layer in the capsule tailoring the density profile at the ablator-ice interface and avoiding preheat of the ice fuel layer. The experimental hohlraum radiation temperatures scale with laser energy and hohlraum size according to the Marshak scaling [17] and are successfully modeled by radiation-hydrodynamic simulations using the code LASNEX [18]. The experimental data and modeling show a radiation drive of 300 eV in an ignition-scale hohlraum with a 2.2 mm-diameter capsule that will allow implosions with sufficient mass for ignition.

The experiments use cryogenic gas-filled gold hohlraums at temperatures of 20 or 24 K containing cryogenic plastic capsules nominally filled to high densities of 8.2 mg cm^{-3} helium. Some capsules also contain traces

of deuterium of up to 30% atom fraction. The hohlraums are 1 cm long with a diameter of 5.44 mm and filled with helium or helium:hydrogen gas at densities of 0.65–1.3 mg cm^{-3}. In addition, experiments with reduced-scale hohlraums (84%) have been performed with length of 8.4 mm, diameter of 4.6 mm, and capsule diameters of 1.85–1.95 mm. The hohlraums are heated with up to 192 frequency-tripled laser beams at a wavelength of 351 nm through two laser entrance holes (LEHs) of 2.94 mm or 3.1 mm-diameter on either end (Fig. 1). The beams are arranged in two cones entering through each LEH; the inner cone being at angles of 23.5° and 30° and the outer cone being at 44.5° and 50° to the vertical axis.

Figure 2 shows the total incident laser power for a hohlraum heated with (1.22 ± 0.03) MJ energy and 400 TW peak power. Also shown are scattering losses due to SRS and SBS, and the total absorbed laser power obtained by subtracting the latter from the incident power. Laser backscattering primarily occurs by the SRS instability on the inner cones of beams while backscatter on the outer cones of beams is negligible.

The total SRS is inferred from the absolute 30–100 keV bremsstrahlung emission measurements with the filter fluorescer x-ray (FFLEX) detector. The spectrum can be fit with a two-temperature distribution [19] indicating a hot electron population with a temperature of 16.5–19 keV

produced by damping of the SRS-driven electron plasma (Langmuir) waves along with a high-temperature component at 50 keV. For the megajoule heated hohlraums, integrating the former and using the Manley-Rowe relations yields a total SRS loss of 100 to 140 kJ (± 15%) while integrating the latter [20,21] results in hot electron energies of 250 to 875 J (± 50%). Combining these findings with the SRS backscatter measurements of 45 kJ using FABS and NBI detectors on the 30° cone indicates a 55 to 95 kJ SRS loss on the 23.5° cone of beams.

Maintaining close to 90% coupling for hohlraums driven by more than 0.5 MJ energy has been the result of optimizing the hohlraum gas fill species, density, and the laser polarization smoothing [22] choice. We have replaced a 20% helium, 80% hydrogen mixture by atomic fraction with a pure He hohlraum gas fill and varied the fill pressure from 1.3 to 0.94 mg cm^{-3}.

In addition, the polarization rotators on the inner cones of beams have been optimized. On NIF, a quad of four f-20 beams enter the target chamber through one effective f-8 optics assembly and overlay on target. Two of these beams are equipped with polarization rotators; these have been arranged into a checkerboard geometry to optimize the overlap of beams with orthogonal polarizations inside the hohlraum. In reduced-scale hohlraum experiments, these improvements have reduced SRS losses by a factor
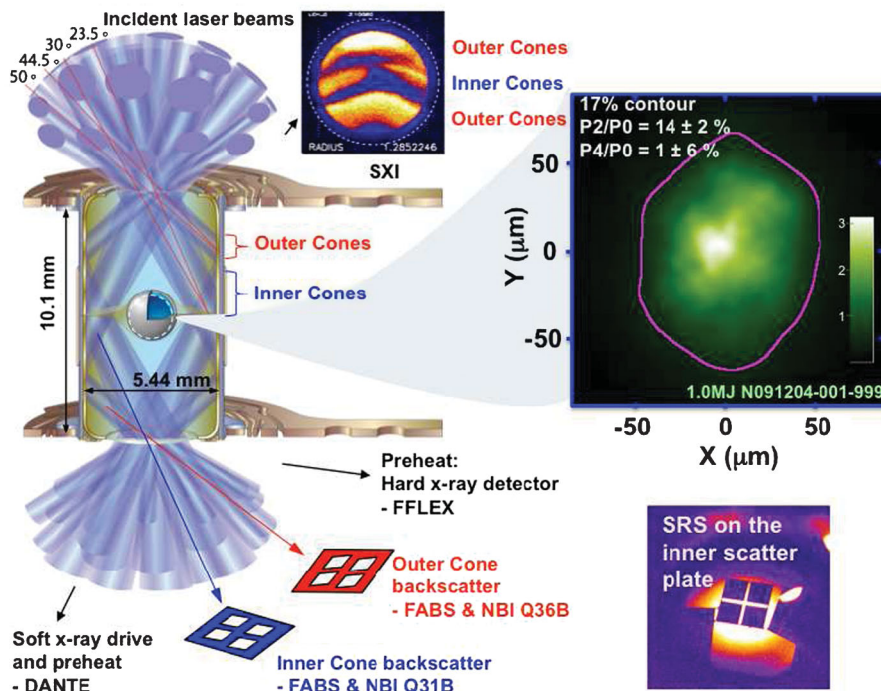

FIG. 1 (color). Schematic of a hohlraum heated by 192 laser beams is shown along with various optical and x-ray diagnostics. Gated x-ray images from implosions driven with megajoule laser energy show symmetric 9 keV capsule x-ray emission at peak compression, 1 to 1.5 ns after the end of the laser pulse. The hohlraum radiation temperature is measured through the LEH with the Dante detector while laser energy and power backscattered from the target is measured with temporally and spectrally resolved backscatter diagnostics using full aperture back scatter (FABS) and near backscatter imager (NBI) detectors on two quads of beams on the 30° and 50° cones.
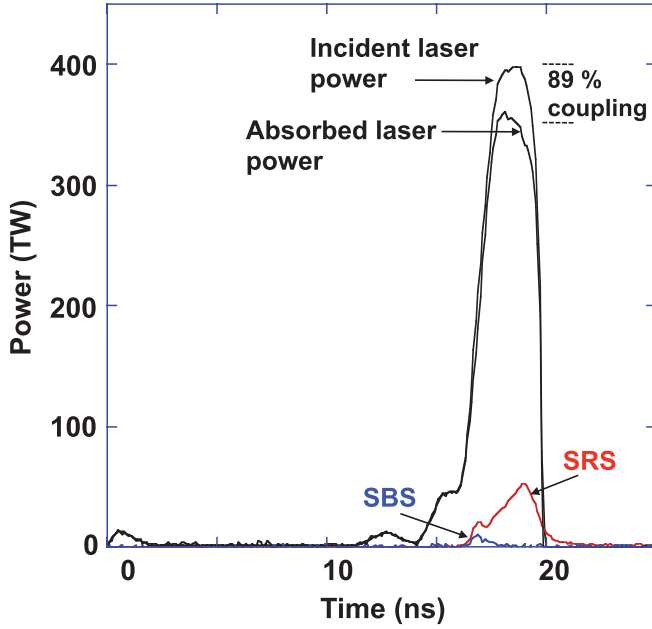
FIG. 2 (color). Measured incident and absorbed laser powers of a 1.22 MJ driven ignition-scale hohlraum shows 89% energy coupling. Also shown are experimental stimulated raman scattering (SRS) and stimulated brillouin scattering (SBS) powers.
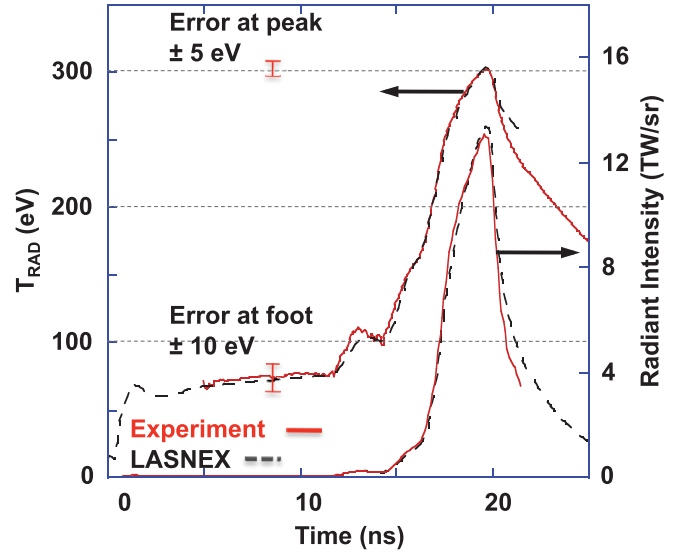

FIG. 3 (color). Experimental and calculated hohlraum radiation temperatures of a 1.2 MJ driven ignition-scale hohlraum are shown as function of time (left scale). Also shown are the measured radiant power, P, from Dante and from radiation-hydrodynamic modeling (right scale).

of 2 at 0.5 MJ and have resulted in 91% and 92% coupling for 11 ns and 16 ns long heater beam pulses. For this scale, the coupling is found 2%–3% lower than previously quoted [10,23] due to improved analysis that include estimates of SRS on the 23.5° cone of beams inferred from the FFLEX measurements.

Figure 3 shows experimental and calculated hohlraum radiation temperatures as function of time. Both the temporal dependence and peak values are in excellent agreement with radiation-hydrodynamic modeling using the code LASNEX. The data are inferred from measurements of the x-ray power, P, in the energy range of $0 < E_{\text{x-ray}} < 20$ keV out of the laser entrance hole (LEH) with the absolutely calibrated broadband x-ray spectrometer Dante [24].

From the measured radiant intensity the temperature can be inferred via $dP/d\Omega = A_{\text{LEH}}(t)\phi(t)\cos\theta\sigma T_{\text{RAD}}^4/\pi$. Here, σ is the Stefan-Boltzmann constant and θ is the view angle of Dante towards the hohlraum axis. The dynamically varying source area, $A_{\text{LEH}}(t)$ is estimated from the 3–5 keV x-ray images [25] of the LEH measured with the static x-ray imager, SXI, cf. Fig. 1. These measurements shows a reduction of the LEH diameter to 83% of the initial value. ϕ is the view factor that relates the Dante measured drive with the radiation temperature seen by the capsule; the latter two factors result in a 10–15 eV corrections for these experiments.

The internal hohlraum radiation temperatures are modeled by balancing the absorbed laser power with the x-ray power radiated into the wall, P_W, absorbed by the capsule, P_{CAP}, and the power that escapes though the LEH, P_{LEH},

$$
\begin{aligned}
\eta_{\text{CE}}(P_L - P_{\text{Backscatter}}) &= P_W + P_{\text{LEH}} + P_{\text{CAP}} \\
&= \sigma T_{\text{RAD}}^4[(1-\alpha_W)A_W + A_{\text{LEH}} \\
&\quad + (1-\alpha_{\text{CAP}})A_{\text{CAP}}].
\end{aligned} \tag{1}
$$

With η_{ce} being the x-ray conversion efficiency from laser power to soft x-rays [26]; α_W and α_{CAP} are the x-ray albedo of the hohlraum wall and the capsule, respectively. The albedo is defined as the ratio of reemitted to incident x rays. The hohlraum wall area, laser entrance hole area, and capsule surface area are denoted by A_W, A_{LEH} and A_{CAP}, respectively.

Figure 4 shows the experimental peak radiation temperatures for various hohlraum experiments as function of the absorbed energy along with results from radiation-hydrodynamic modeling with the code LASNEX that uses the detailed configuration accounting model for x-ray opacities [27,28]. Generally, we observe good agreement between data and modeling, in particular, at ignition scale we have achieved a hohlraum drive of 300 eV at 1.1 MJ absorbed energy. Also shown in Fig. 4 are the Marshak scaling results [17] of Eq. (1) assuming a conversion efficiency of $\eta_{\text{ce}} = 0.9$ and the albedo calculated according to [29]. The latter increases according to the data and integrated modeling and provides a good match to the experimental data at both hohlraum scales.

For seven experiments with 1 to 1.08-MJ laser energy delivered to the hohlraum, the radiation temperature varies from 279 to 288 eV with an absolute error bar of 5 eV. These data indicate a reproducible temperature with a standard deviation of approximately 3 eV in temperature
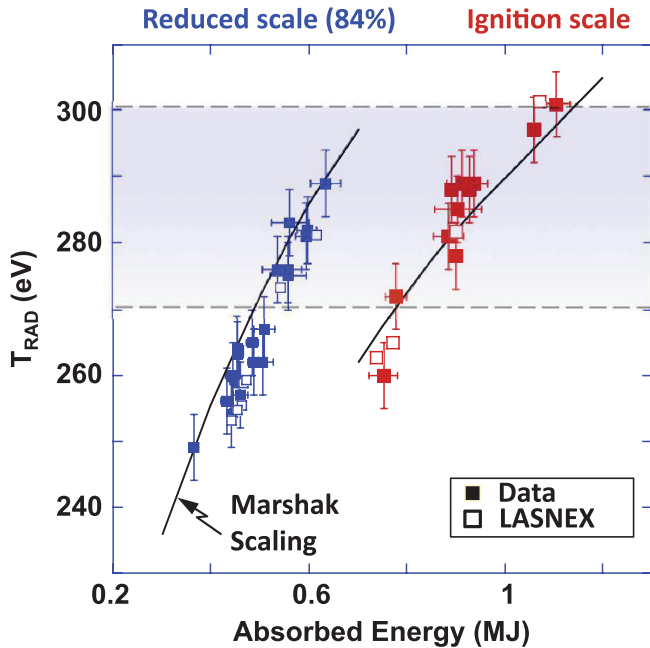
FIG. 4 (color). Experimental and calculated hohlraum radiation temperatures are shown as function of the absorbed laser energy. The measured values are from the broadband x-ray spectrometer Dante and radiation-hydrodynamic modeling using the code LASNEX with detailed configuration accounting. The Marshak scaling equates the absorbed laser power with a x-ray conversion efficiency of 90% with radiation losses according to Eq. (1). The results demonstrate $T_{RAD} = 300$ eV ignition hohlraum temperature at ≥ 1.1 MJ of absorbed laser energy.

fusion capsule implosions. The experiments show a radiation temperature of 300 eV with 87% to 91% coupling of the incident laser energy. The data scale with radiation temperature according to radiation-hydrodynamic calculations and modeling. Future studies will explore further improvements in hohlraum drive including experiments with optimized wall areas and hohlraum fill densities as well as hohlraums with higher-Z wall materials and higher wall opacities [30–32], e.g., uranium.

and 4% for the radiant intensity. These results meet the requirements for the ignition point design. In addition, these shots consistently show good symmetry. The soft x-ray flux asymmetry at the capsule is decomposed into Legendre polynomials, P_n. Odd orders ($n = 1, 3, \ldots$) are approximately zero due to the up-down illumination symmetry and low-order even modes ($n = 2, 4$) are the most important asymmetries. Higher order drive variations are negligibly small and smoothed by the hohlraum radiation environment. Here, the megajoule experiments show $P_2/P_0 < 0.25$ cf. Fig. 1, which combined with the wavelength tuning capability, is adequate for ignition.

Further, including the fact that hohlraum wall loss scales as $P/A_W \times t^{0.6}$, Eq. (1) reproduces the observed constant T_{RAD} for the increased hohlraum wall area and pulse duration.

In summary we have demonstrated efficient heating of ignition-scale hohlraums with radiation temperature and illumination symmetry required for inertial confinement

[1] E. Moses and C. R. Wuest, Fusion Sci. Technol. **47**, 314 (2005).
[2] C. Haynam et al., Appl. Opt. **46**, 3276 (2007).
[3] S. W. Haan et al., Phys. Plasmas **2**, 2480 (1995).
[4] J. D. Lindl, Phys. Plasmas **2**, 3933 (1995).
[5] J. D. Lindl et al., Phys. Plasmas **11**, 339 (2004).
[6] S. Atzeni, J. Meyer-ter-Vehn, *The Physics of Inertial Fusion* (Oxford Univ. Press, New York, 2004).
[7] A. A. Hauer et al., Phys. Plasmas **2**, 2488 (1995).
[8] O. L. Landen et al., Phys. Plasmas **6**, 2137 (1999).
[9] R. E. Turner et al., Phys. Plasmas **7**, 333 (2000).
[10] S. H. Glenzer et al., Science **327**, 1228 (2010).
[11] P. Michel et al., Phys. Plasmas **17**, 056305 (2010).
[12] L. J. Suter et al., Phys. Rev. Lett. **73**, 2328 (1994).
[13] W. J. Krauser, Phys. Plasmas **3**, 2084 (1996).
[14] S. H. Glenzer et al., Phys. Rev. Lett. **80**, 2845 (1998).
[15] R. Betti et al., Phys. Plasmas **17**, 058102 (2010).
[16] P. Chang et al., Phys. Rev. Lett. **104**, 135002 (2010).
[17] R. E. Marshak, Phys. Fluids **1**, 24 (1958).
[18] G. B. Zimmerman and W. L. Kruer, Comments Plasma Phys. Controlled Fusion **2**, 51 (1975).
[19] C. A. Thomas, Phys. Rev. E **81**, 036413 (2010).
[20] K. A. Brueckner, Phys. Rev. Lett. **37**, 1247 (1976).
[21] R. P. Drake et al., Phys. Rev. A **40**, 3219 (1989).
[22] E. Lefebvre et al., Phys. Plasmas **5**, 2701 (1998).
[23] N. Meezan et al., Phys. Plasmas **17**, 056304 (2010).
[24] E. L. Dewald et al., Rev. Sci. Instrum. **75**, 3759 (2004).
[25] M. B. Schneider et al., Rev. Sci. Instrum. **81**, 10E538 (2010).
[26] E. Dattolo et al., Phys. Plasmas **8**, 260 (2001).
[27] J. L. Kline et al., Phys. Rev. Lett. **106**, 085003 (2011).
[28] R. P. J. Town et al., Phys. Plasmas (to be published).
[29] R. Sigel et al., Phys. Rev. Lett. **65**, 587 (1990).
[30] R. E. Olson et al., Rev. Sci. Instrum. **74**, 2186 (2003).
[31] J. Schein et al., Phys. Rev. Lett. **98**, 175003 (2007).
[32] O. S. Jones et al., Phys. Plasmas **14**, 056311 (2007).